JACS
JOURNAL OF THE AMERICAN CHEMICAL SOCIETY
Article
pubs.acs.org/JACS

Synergy of Two Assembly Languages in DNA Nanostructures: Self-Assembly of Sequence-Defined Polymers on DNA Cages

Pongphak Chidchob, Thomas G. W. Edwardson, Christopher J. Serpell, and Hanadi F. Sleiman*

Department of Chemistry and Centre for Self-Assembled Chemical Structures (CSACS-CRMAA), McGill University, 801 Sherbrooke Street West, Montreal, Quebec H3A 0B8, Canada

Supporting Information

ABSTRACT: DNA base-pairing is the central interaction in DNA assembly. However, this simple four-letter (A−T and G−C) language makes it difficult to create complex structures without using a large number of DNA strands of different sequences. Inspired by protein folding, we introduce hydrophobic interactions to expand the assembly language of DNA nanotechnology. To achieve this, DNA cages of different geometries are combined with sequence-defined polymers containing long alkyl and oligoethylene glycol repeat units. Anisotropic decoration of hydrophobic polymers on one face of the cage leads to hydrophobically driven formation of quantized aggregates of DNA cages, where polymer length determines the cage aggregation number. Hydrophobic chains decorated on both faces of the cage can undergo an intrascaffold "handshake" to generate DNA-micelle cages, which have increased structural stability and assembly cooperativity, and can encapsulate small molecules. The polymer sequence order can control the interaction between hydrophobic blocks, leading to unprecedented "doughnut-shaped" DNA cage-ring structures. We thus demonstrate that new structural and functional modes in DNA nanostructures can emerge from the synergy of two interactions, providing an attractive approach to develop protein-inspired assembly modules in DNA nanotechnology.

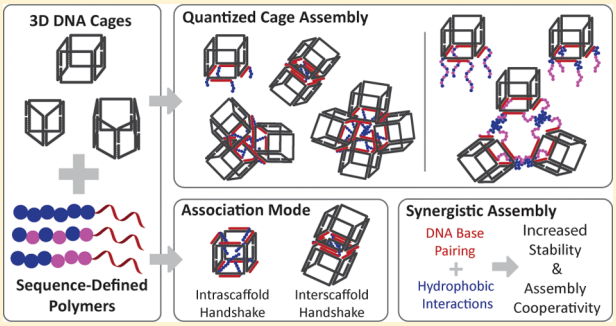

INTRODUCTION

Sequence-controlled polymers, such as oligonucleotides and polypeptides, are remarkable macromolecules in which the order of the building blocks along the polymer chain provides all necessary instructions for efficient structural control, molecular recognition, and catalysis.[1] In particular, polypeptide chains are programmed to fold themselves into final predetermined structures with very high accuracy to construct important biological nanomachines. Although such a level of structural and functional complexity has not been fully realized synthetically,[1] the field of DNA nanotechnology offers a powerful tool to create finely designed two- and three-dimensional architectures and devices by using DNA as the main building block.[2−11] However, a large number of DNA strands of unique sequences are generally required for the assembly of more complex structures. This decreases scalability and can theoretically increase assembly errors, due to the limited four-letter A−T and G−C "language" in DNA assembly.

The incorporation of multiple molecular interactions within the same building block is an efficient strategy to achieve complex and hierarchical assembly in biological systems. Of these, hydrophobic interactions are the underlying mechanism for many structural elements in biology such as phospholipid bilayers, vesicles, and many proteins. They are also a fundamental driving force for the self-assembly of synthetic block copolymers into various morphologies such as spherical micelles, cylindrical micelles, and vesicles.[12] The integration of hydrophobic interactions with DNA base-pairing is a promising approach not only to overcome the complexity−scalability−error issues but also to introduce new assembly modes and functionalities in DNA assembly.[13,14] Inspired by protein folding, we would like to create assembly modules, such as protein coiled-coil motifs, as elementary repeats in DNA nanotechnology; thus, we need to understand the rules governing the interplay between the two languages in the assembly. However, one of the problems is the difficulty in the synthesis of DNA conjugated with hydrophobic molecules and polymers. Our group has recently developed an automated solid-phase synthesis to prepare monodisperse DNA-polymer conjugates based on phosphoramidite chemistry.[15] This approach not only is convenient, rapid, and high yielding but also allows one to place functional monomers in a sequence-controlled manner on the polymer backbone.

The combination of DNA base-pairing with hydrophobic interactions can expand assembly modes to DNA nanostructures which would not be possible otherwise. DNA cages have emerged as a promising platform for cellular delivery of therapeutics.[16−20] However, unmodified DNA/RNA structures

Received: December 11, 2015
Published: March 21, 2016

DOI: 10.1021/jacs.5b12953
J. Am. Chem. Soc. 2016, 138, 4416−4425

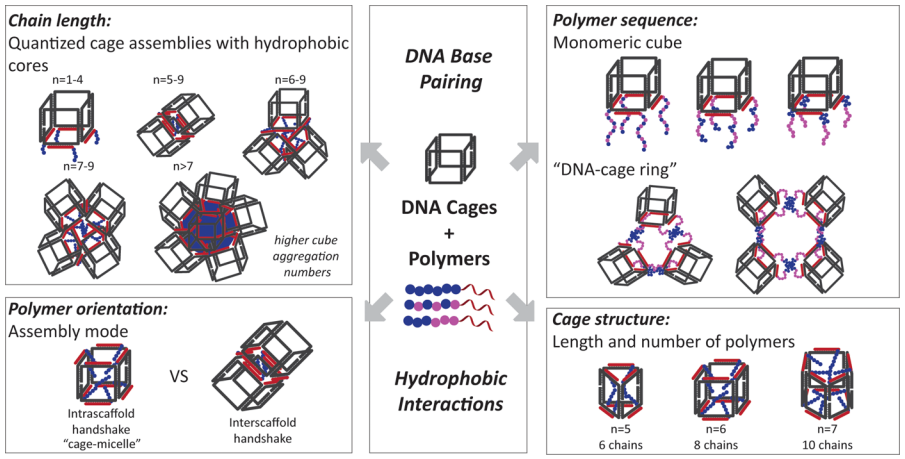

Figure 1. Schematic representation of the self-assembly of sequence-defined hydrophobic polymers on DNA cages. The blue and magenta circles denote hydrophobic and hydrophilic monomers along the polymer chains, where 'n' is the number of hydrophobic repeats. (Top Left) Hydrophobic polymers on one face of DNA cage lead to "quantized cage assemblies", whose aggregation number depends on the number of hydrophobic repeats. (Top right) Depending on their sequence, polymers with hydrophilic and hydrophobic repeats give monomeric cages, or donut-shaped "cage-rings". (Bottom left) When both faces of the DNA cage have hydrophobic polymers, they can undergo an intrascaffold "handshake" into a "cage-micelle" that encapsulates small molecules and is significantly more stable than the unsubstituted cage. (Bottom right) Depending on cage geometry, the intrascaffold "handshake" occurs with a different number of hydrophobic repeats, with a different capacity for small molecules.

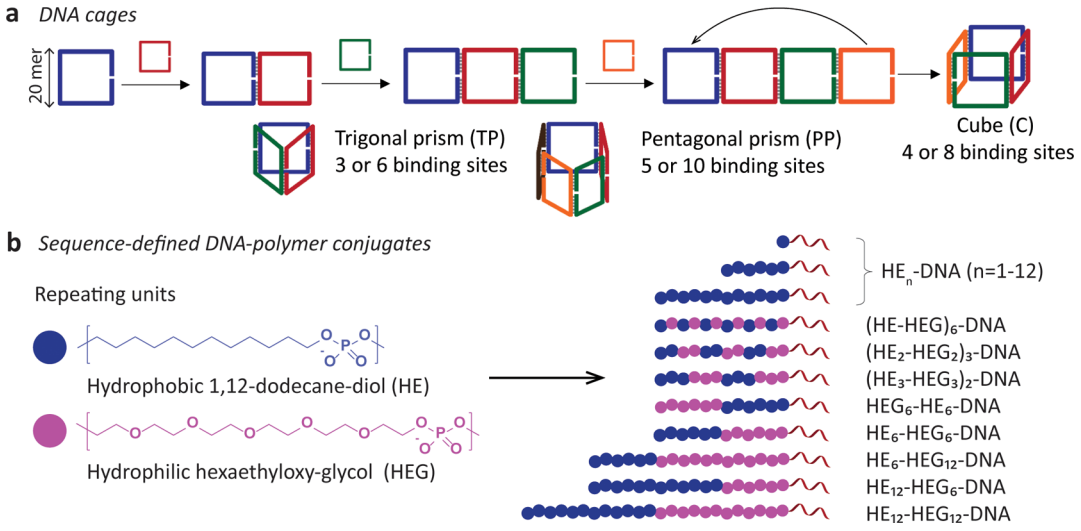

Figure 2. Cage and DNA–polymer conjugate design. (a) Clip-by-clip approach for DNA cage construction. A cube can be constructed from four different 80-mer DNA clips and contains a maximum of eight binding sites. (b) Hydrophilic hexaethyloxy-glycol (HEG) and hydrophobic 1,12-dodecane-diol (HE) monomers for the synthesis of sequence-defined DNA–polymer conjugates. The 14-mer single-stranded DNA can hybridize to the single-stranded segments on the cages.

suffer from nuclease instability, poor cellular penetration, and rapid clearance *in vivo*.[16−20] Attaching hydrophobic functionalities and increasing the assembly range of DNA cages can be an effective method to overcome these barriers. To our knowledge, the implementation of hydrophobic interactions in the design of DNA nanostructures is still considerably unexplored. Some examples that integrate hydrophobic interactions with DNA nanostructures include self-folding of DNA rectangles mediated by cholesterol[21] and hydrophobic dendritic molecules,[22] and DNA tetrahedra functionalized with a thermoresponsive polymer that can transition between a discrete tetrahedron and giant-surfactant aggregates.[23] Recent work by our group has demonstrated the significant role of hydrophobic interactions in directing the association of alkyl chains on three-dimensional DNA scaffolds. The number and position of the chains on DNA cubes can dramatically alter their assembly behavior.[14,24]

In this article, we report an in-depth study of the self-assembly of sequence-defined hydrophobic polymers on DNA cages (Figure 1). Our system allows the systematic change of cage structure and size, and orientation of individual polymer chains on the DNA scaffold. On the polymer end, the polymers are monodisperse and sequence controlled in such a way that we can precisely change the number of hydrophobic repeats, the relative number of hydrophilic to hydrophobic repeats, and the polymer sequence. We found that decoration of the polymers on the cages leads to new DNA superstructures through hierarchical assembly, via DNA base-pairing and hydrophobic interactions (Figure 1). (i) Short hydrophobic chains result in *monomeric DNA cage structures*. (ii) Intermediate chains arranged on one face of the DNA cage

DOI: 10.1021/jacs.5b12953
J. Am. Chem. Soc. 2016, 138, 4416−4425

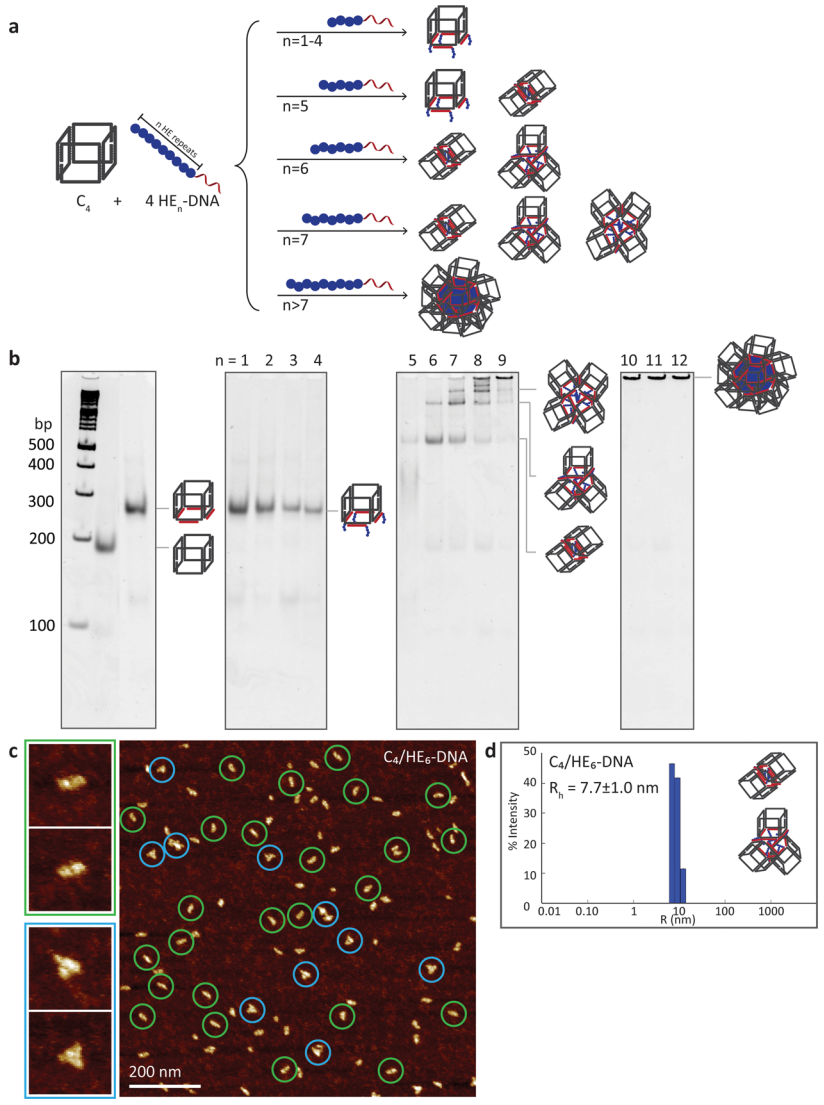

Figure 3. Decoration of one face of C_4 with four HE_n-DNA (n = 1−12). (a) Assembly products of C_4 with HE_n-DNA. Finite cube aggregation number that scales with the number of hydrophobic HE repeats are observed. (b) Native PAGE showing the assembly of C_4, C_4/DNA, and C_4/HE_n-DNA. (c) AFM image of C_4/HE_6-DNA showing cube dimers (green circles) and cube trimers (blue circles). (d) Size distribution histogram of C_4/HE_6-DNA obtained from DLS (see Supplementary Figure 26 for additional AFM images).

result in *quantized cage assemblies*, where a specific number of DNA cages is organized around a hydrophobic core; here, the number of repeats in the polymer defines the size of the hydrophobic core and dictates the number of DNA cages that form these aggregates. (iii) Hydrophobic chains on both faces of the cage undergo an intrascaffold "handshake", to give *DNA-micelle cages*. Hydrophobic interactions not only mediate the encapsulation of small molecules in the cage but also significantly increase structural stability and assembly cooperativity. (iv) Specific polymer sequences result in unprecedented *doughnut-shaped DNA cage-ring structures*, where DNA cages are organized into rings, whose diameter and density can be controlled by varying the length of the polymer blocks. We propose a mechanism for the hydrophobically driven quantized self-assembly that is dependent on the chain length of the polymers, and we study the dynamic ability of the quantized DNA cage assemblies to undergo structural exchange. We thus demonstrate the efficient use of sequence-defined hydrophobic polymers to create orthogonal assembly modes which synergistically combine hydrophobic and base-pairing interactions in the assembly of DNA nanostructures.

RESULTS AND DISCUSSION

Design of DNA Cages and Sequence-Defined DNA–Polymer Conjugates. DNA cages were chosen as scaffolds for three-dimensional positioning of DNA–polymer conjugates and were assembled via a "clip-by-clip" approach.[14,24] The clips are 80-mer DNA strands composed of four single-stranded segments separated by a hexaethyloxy-glycol (HEG) spacer. The 20-mer segment in the middle of the clip can hybridize to two peripheral 10-mer segments of the next clip. Cube (C) can be constructed from four clips where the fourth clip folds back and hybridizes to the first clip, cyclizing the cubic assembly (Figure 2a). This structure presents eight 20-mer segments that are single-stranded and provides binding sites for DNA–polymer conjugates. In a similar approach, trigonal prism (TP) and pentagonal prism (PP) can be generated from three and five clips, respectively, and structures were generated in

DOI: 10.1021/jacs.5b12953
J. Am. Chem. Soc. 2016, 138, 4416–4425

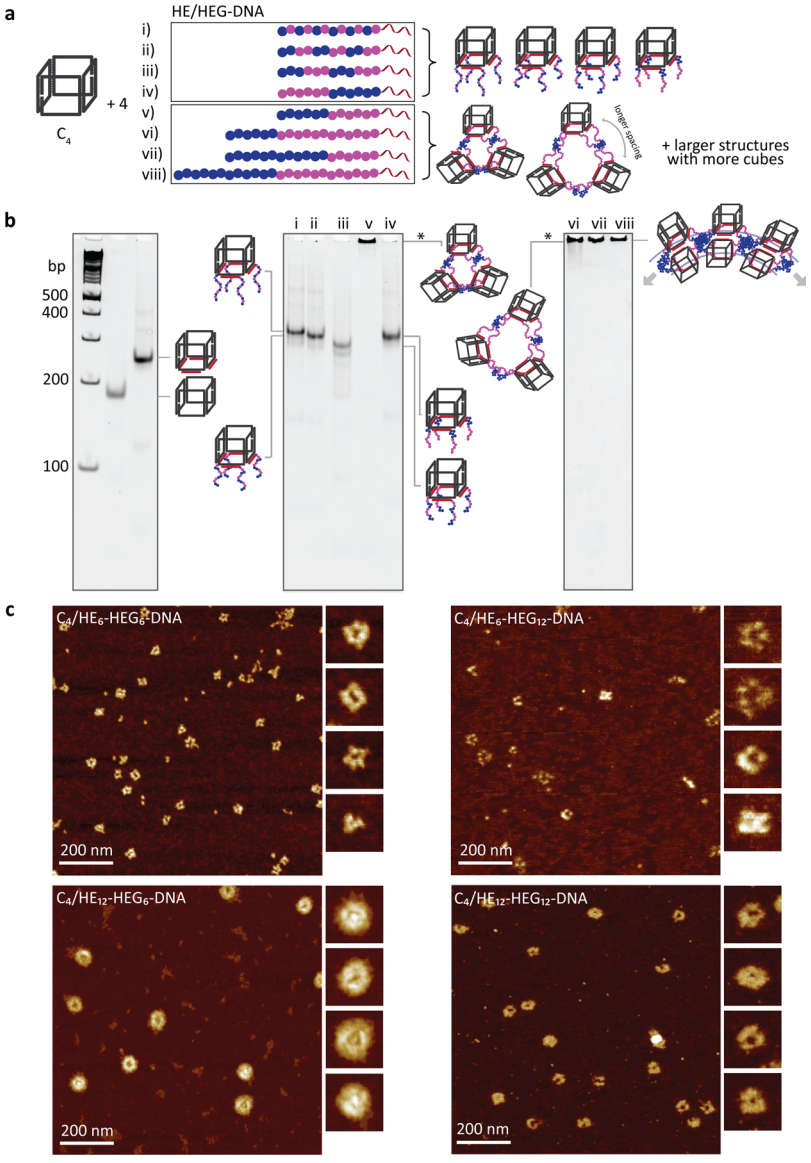

Figure 4. Decoration of C_4 with four HE/HEG-DNA. (a) Assembly products of C_4 with HE/HEG-DNA. The polymer sequences can dictate whether the assembly either yields a monomeric cube or forms higher-order structure. (b) Native PAGE showing the assembly of C_4, C_4/DNA, C_4 with HE/HEG-DNA. *Only the schematics of rings with 3 vertices were shown here for C_4/HE_6-HEG_6-DNA and C_4/HE_6-HEG_{12}-DNA. (c) AFM images of C_4 with HE_n-HEG_m-DNA (n = 6, 12 and m = 6, 12). The presence of HEG block in the polymer chains can increase the spacing between the cubes.

quantitative or near-quantitative yields (see Section V in Supporting Information).

To prepare sequence-defined DNA-polymer conjugates, 1,12-dodecane-diol (hexaethylene, HE) and hexaethyloxy-glycol (HEG) were chosen as hydrophobic and hydrophilic monomers (Figure 2b). These monomers were attached to a 19-mer DNA by automated solid-phase synthesis using phosphoramidite chemistry.[15] The DNA segments contain a 5T spacer and 14-mer complementary sequence to the single-stranded segments on the cages. A series of DNA-HE conjugates and DNA-HE/HEG copolymer conjugates were synthesized to systematically investigate the design parameters of DNA-polymer conjugates for their assembly behavior on DNA cages (Figure 1b, and see Section IV in Supporting Information).

Polymers: Number of Hydrophobic Repeats. We had previously decorated DNA cubes with dendritic alkyl chains and showed that a cube with four dendritic chains on one of its faces can associate into a dimer via an interscaffold "handshake" of the hydrophobic repeats.[14] We also introduced hydrophobic polymers HE_n-DNA (Figure 2b) on one face of a DNA cube and preliminarily showed their assembly into discrete aggregates, which we hypothesized to be cube dimer, tetramer, hexamer, etc.[24] With a very long alkyl component in HE_n-DNA (n = 12) on one face of a DNA cube, we showed the formation of a spherical micelle with a hydrophobic core, and DNA cubes on its exterior. This cube micelle displayed dynamic character (cubes can be removed by strand displacement) as well as the ability to form higher-order micelle networks and to act as a scaffold to organize fluorescent dyes into an antenna structure with controlled FRET.[24]

To develop a better understanding of the rules for this hydrophobically driven assembly, it was crucial to further characterize the molecularity of the quantized cage aggregates.

DOI: 10.1021/jacs.5b12953
J. Am. Chem. Soc. 2016, 138, 4416−4425

We thus examined the effect of the chain length of hydrophobic polymers HE_n-DNA on their assembly with DNA cages (Figure 3a, we name the DNA sequence on the polymer "DNA"). Cube C_4 has four identical single-stranded stretches on one of its faces, each complementary to the DNA strand of the DNA–polymer conjugates. The decoration of C_4 with four HE_n-DNA was achieved by mixing all components in magnesium-containing buffer and then thermally annealing from 95 to 4 °C over 4 h. The formation of DNA nanostructures was followed by native polyacrylamide gel electrophoresis (PAGE) as shown in Figure 3b. Addition of four complementary unmodified DNA strands to C_4 yielded a single band of lower electrophoretic mobility. Addition of strands with short hydrophobic chains to one face of cube C_4, from HE_1-DNA to HE_4-DNA, resulted in single bands of similar electrophoretic mobility compared to C_4 with unmodified DNA, consistent with a monomeric cube. The lack of difference in electrophoretic mobility for these cubes as the number of hydrophobic repeats in HE_n-DNA increases (n = 1–4) is possibly consistent with some chain folding or interaction of these chains across one face of the cube in a manner that does not impede the movement of the assemblies on native PAGE. Thus, when DNA–polymer conjugates with 1–4 hydrophobic repeats were added to one face of the cube, monomeric structures decorated with hydrophobic groups are formed.

When longer hydrophobic chains from HE_5-DNA to HE_{12}-DNA were added to C_4, we no longer see the monomeric cube as a major product. Instead, we observe the combination of cubes into discrete aggregates. This is likely due to the increased hydrophobicity of the polymer chains attached to the cube, promoting cube association to hide these hydrophobic chains in the core (akin to a protein coiled-coil motif). The identity of C_4/HE_6-DNA was elucidated by atomic force microscopy (AFM). Figure 3c reveals elongated structures of two spheres, which accounted for 76% of population (cube dimers), and triangular structures with the edge length of ∼30 nm (cube trimers, see below). Some disaggregation of the higher-order structures into individual cubes (diameter of ∼17–18 nm) was also noted on the mica surface and can be attributed to strong electrostatic interactions between DNA and mica, which compete with the hydrophobic interactions holding together the DNA nanostructures.[21] The hydrodynamic size measured by dynamic light scattering (DLS) indicates that C_4/HE_6-DNA had low polydispersity, but was not able to differentiate between the two populations of higher-order structures (Figure 3d, and see Section XIX in Supporting Information for isolation of the individual higher-order structures).

To further support the identity of C_4/HE_6-DNA, we tagged each cube with a gold nanoparticle (see Section VIII in Supporting Information) and preliminarily characterized the assemblies by transmission electron microscopy (TEM). We observed a larger population of the clusters containing 2 and 3 AuNPs in close proximity (see Supplementary Figure 15). The technique was complicated by sample–surface interactions, which sometimes resulted in populations of higher-order aggregates. However, these observations are consistent with dimeric and trimeric structures as the identity of the higher-order structures for C_4/HE_6-DNA.

As the number of hydrophobic HE repeats on the polymer increased, increasingly large superstructures were formed. Interestingly, their aggregation number correlated with the number of HE repeats. Comparison of these bands to the DNA ladder allowed an estimation of relative "molecular weight" for each higher-order structure, and we can calculate a cube aggregation number by comparing these molecular weights to that of the monomeric structure. The results suggest that the cube aggregation number gradually increases by increments of one (see Section VII in Supporting Information). Thus, HE_7-DNA gives dimer, trimer, and tetramer, and HE_8-DNA gives trimer, tetramer, and pentamer. HE_9-DNA to HE_{12}-DNA give nonpenetrating bands, which may be composed of incrementally higher cube aggregation numbers. However, it should be noted that the relationship between cube aggregation number and electrophoretic mobility can also be nonlinear.

Polymers: Sequences of the Polymers and Relative Numbers of Hydrophilic to Hydrophobic Repeats. The monomer sequence along polymer chains can significantly influence polymer physical properties. To investigate this effect on DNA cages, we assembled cube C_4 with a series of copolymers of different sequences, all containing a constant number of six hydrophobic HE and six hydrophilic HEG repeats per chain. This includes alternating chains of single monomers $(HE\text{-}HEG)_6$-DNA, two monomers $(HE_2\text{-}HEG_2)_3$-DNA, three monomers $(HE_3\text{-}HEG_3)_2$-DNA, and six monomers (Figure 4a). The latter polymer has two sequences: $HEG_6\text{-}HE_6$-DNA, in which the hydrophobic portion is between the DNA and HEG chains, and $HE_6\text{-}HEG_6$-DNA, in which the hydrophobic portion is at the chain end. Only the latter structure among this copolymer series was previously shown to assemble into micellar aggregates, whereas the other structures remain as unimers in solution.[15]

Decoration of these HE/HEG-DNA polymers on cube C_4 yielded monomeric structures (Figure 4b, with one exception, see below). The electrophoretic mobility of these structures on native PAGE increased with HE block length, consistent with greater structure compaction. As the HE block becomes longer, the local hydrophobicity of individual HE segments increases, thus potentially enabling more efficient folding of the hydrophobic chains, which can make the structures increasingly compact and increases their gel mobility. Interestingly, these polymers did not result in cube aggregation, despite their relatively high hydrophobic content. These cages are especially interesting for applications in cellular delivery: they behave as monomers, yet their hydrophobic content can facilitate interaction with cellular membranes and modify their delivery profile.[18,19,25,26] It is of note that this behavior is a direct result of sequence control of the polymers, where regular block copolymers would not be able to generate this property.

The exception to this monomeric assembly was $C_4/HE_6\text{-}HEG_6$-DNA, which gave higher-order structures that appeared as a nonpenetrating band on the native PAGE. The AFM images (Figure 4c) reveal polygonal rings containing 3–5 vertices with an edge length of ∼30 nm. The size of the structures was also supported by DLS measurements (R_h = 14 nm). We believe that the flexible HEG block is able to serve as a spacer between hydrophobic HE domains and the cubes. The HE block of $HE_6\text{-}HEG_6$-DNA can form hydrophobic domains by interacting with the chains on the other cubes side-to-side, resulting in polygonal rings (Figure 4a). As the HEG block might be a crucial parameter for the diameter of the ring-like structures, we hypothesized that a longer HEG block could create structures with larger spacing between the cubes. The hydrodynamic radius of $C_4/HE_6\text{-}HEG_{12}$-DNA (18 nm) was indeed significantly larger than that of $C_4/HE_6\text{-}HEG_6$-DNA. However, in this case, we also observed disassembly of some of

DOI: 10.1021/jacs.5b12953
J. Am. Chem. Soc. 2016, 138, 4416–4425

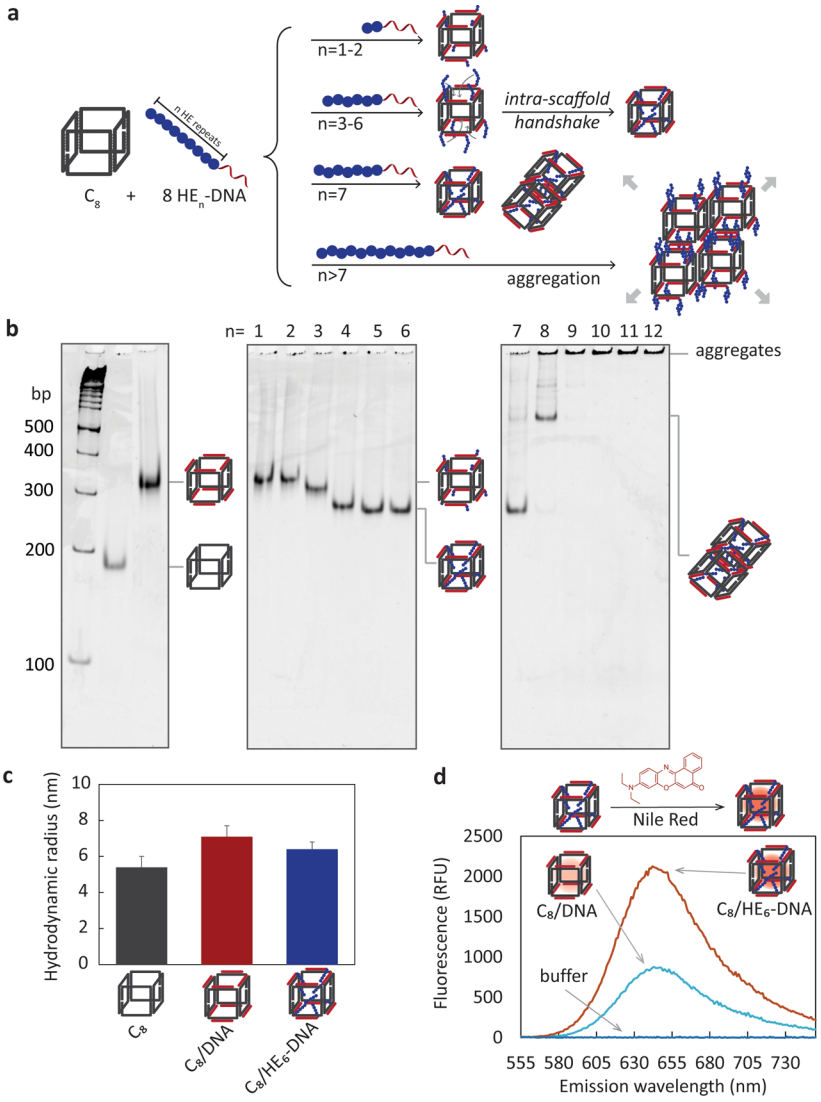

Figure 5. C_8 assembly with HE_n-DNA (n = 1,12) on its two faces. a) Assembly products of C_8 with HE_n-DNA. Medium chain length of hydrophobic polymers (n = 3−6) prefers intrascaffold "handshake" and create hydrophobic core inside the cube. b) Native PAGE showing the assembly products of C_8, C_8/DNA and C_8/HE_n-DNA. c) Hydrodynamic radii of C_8, C_8/AT (7.1 ± 0.6 nm) and C_8/HE_6-AT (6.4 ± 0.4 nm). d) Fluorescent traces of Nile Red molecules encapsulated inside C_8/DNA and C_8/HE_6-DNA. The signal of Nile Red was higher in the presence of HE_6-AT. No fluorescent signal was observed in the buffer (see Section XIV in Supporting Information for details). These observations suggest the formation of hydrophobic core inside the cube.

the structures on the mica surface by AFM, which is likely due to the larger hydrophilic-to-hydrophobic content of this polymer (Figure 4c).

To further increase the stability of this hydrophobic interscaffold "handshake", we assembled C_4/HE_{12}-HEG_6-DNA, which has a longer hydrophobic HE block than C_4/HE_6-HEG_6-DNA. This molecule generated a high yield of well-defined doughnut-shaped structures with hollow features in the middle as observed by AFM (Figure 4c). Further increasing the length of the HEG block to C_4/HE_{12}-HEG_{12}-DNA also showed efficient formation of ring structures, which looked less dense by AFM. The radii of both structures were comparable (20 nm/27 nm (DLS/AFM) for C_4/HE_{12}-HEG_6-DNA; 21/24 nm (DLS/AFM) for C_4/HE_{12}-HEG_{12}-DNA, Figure 4c and see Section XI in Supporting Information for DLS). TEM characterization also confirmed the presence of relatively homogeneous spherical structures (radius 12 nm for C_4/HE_{12}-HEG_6-DNA and 15 nm for C_4/HE_{12}-HEG_{12}-DNA, see Section XIII in Supporting Information). It should be noted that the sizes obtained from AFM and DLS were similar to one another and were significantly larger than those obtained by TEM, suggesting that the structures may be ring-like in solution. The possible explanation for the smaller sizes measured by TEM is a collapse of the structures on the hydrophobic carbon-coated grids and the drying of DNA structures under high vacuum.[27]

The estimated yields of the ring structures obtained by examination of the AFM images were high in all cases, except for the sequence in which the HE block is short (6 units) as compared to the HEG block (12 units). Thus, we can conclude that the addition of HEG repeats provides a spacer between DNA scaffolds and yields ring structures. To our knowledge, the assembly of DNA cages into doughnut-shaped ring structures is unprecedented. It is interesting that, despite the flexibility of both HE and HEG chains, we observed discrete cube assemblies here, rather than linear oligomers.

DOI: 10.1021/jacs.5b12953
J. Am. Chem. Soc. 2016, 138, 4416−4425

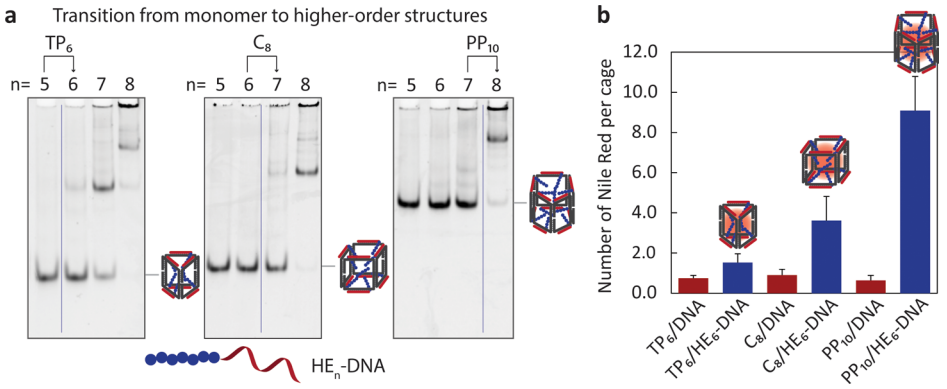

Figure 6. Effect of the cage's structure. (a) Native PAGE showing the assembly products of trigonal prism TP_6, cube C_8, and pentagonal prism PP_{10} with HE_5-DNA to HE_8-DNA. Larger cages could provide more space for the hydrophobic core and therefore can accommodate longer HE_n-DNA without forming higher-order structures (HE_5-DNA for TP_6, HE_6-DNA for C_8, and HE_7-DNA for PP_{10}). (b) Nile Red encapsulation in double-stranded cages (red bars) and cages decorated with HE_6-DNA (blue bars). There was an ~2.5-fold increase in loading capacity with increased cage size.

Cages: Orientation of the Polymer Chains on the Cages. We previously reported that eight dendritic HE chains attached on both faces of a DNA cube result in an intrascaffold association, with the ability to encapsulate molecules in the internal hydrophobic environment.[14] We were interested in probing the dependence of this phenomenon on polymer architecture and chain length (e.g., how many hydrophobic chains can fit inside the cage?). Cube C_8 was designed to allow decoration with up to eight polymer chains on both its top and bottom faces (Figure 5a). A one-pot assembly of C_8 with HE_n-DNA was performed. In Figure 5b, short HE chains generated monomeric structures with a sharp band on the gel. Interestingly, as the number of hydrophobic repeats increased, the electrophoretic mobility of this band increased (rather than decreased); it then remained constant at HE_4-DNA until HE_6-DNA. The structure of C_8/HE_6-DNA was characterized by AFM, which revealed mostly single spherical features with a radius of 9.6 nm, comparable to C_8 (see Supplementary Figures 32 and 33). DLS measurements (Figure 5c) indicated that C_8/HE_6-DNA (R_h = 6.4 ± 0.3 nm) was smaller than C_8/DNA (R_h = 7.1 ± 0.6 nm). A likely assembly mode here is that HE chains (HE_4–HE_6) collapse and create a hydrophobic core inside the cube, resulting in a more compact structure similar to that of dendritic HE chains.[14] The formation of the hydrophobic core in C_8/HE_6-DNA was further supported by the encapsulation of hydrophobic Nile Red fluorescent dye.[28] Compared to a cube decorated with unmodified DNA, there was a significantly higher fluorescent signal of Nile Red in C_8/HE_6-DNA (Figure 5d).

As the number of hydrophobic repeats on the polymer increased, HE_7-DNA started to form a cube dimer and longer hydrophobic chains resulted in higher-order structures as the major product. Thus, up to six HE repeats per polymer chain can be accommodated in the cube core (a total of 48 HE chains), beyond which interscaffold assembly sets in. Both AFM and DLS measurements suggested that extended structures formed in the case of C_8/HE_8-DNA and C_8/HE_{12}-DNA (see Sections XI and XII in Supporting Information for DLS and AFM).

Cages: Structures and Sizes of the Cages. The clip-by-clip approach allows the efficient construction of cages with various geometries and sizes. This geometric variation offers more design parameters to control the number and the orientation of the polymers on the cages. It allows us to answer the question: can the cage geometry change the onset of assembly and the number of cages per agggregate? To investigate this effect, trigonal prism (TP) and pentagonal prism (PP) were assembled with HE_n-DNA in an analogous way to the cube C/HE_n-DNA. With these chains on one face of the cage, the hydrophobically driven aggregation numbers for TP_3 and PP_5 were indeed different from those of the cube C_4. With HE_6-DNA on one face, TP_3 gave a dimer, trimer, and tetramer while C_4 and PP_5 gave only a dimer and trimer (see Supplementary Figures 6 and 7 for TP_3 and PP_5). This can be explained by the smaller size of the trigonal prism, allowing more cages to fit around the hydrophobic core. Thus, the aggregation number can be tuned with the cage geometry.

With HE_n-DNA on both faces, we expect that the smaller trigonal prism can accommodate shorter polymer chains in its core than the cube, and the pentagonal prism would encapsulate larger polymer chains. Indeed, TP_6 could accommodate lengths up to HE_5 within its core (capacity 30 HE repeats), before the cage started to dimerize with HE_6; this transition occurred from HE_6 to HE_7 for the cube (capacity 48 HE repeats) and from HE_7 to HE_8 for the pentagonal prism (capacity 70 HE repeats, Figure 6a). The larger cages and higher total number of HE repeats per cage can in principle increase the loading capacity of hydrophobic guests. To verify this, we compared the loading capacity of the three different cages decorated with HE_6-DNA (Figure 6b). The results showed an approximately 2.5-fold increase in Nile Red loading capacity when the size of cages and thus total number of HE_6-DNA increased: 9.1 ± 1.7 molecules per PP_{10}/HE_6-DNA, 3.6 ± 1.2 molecules per C_8/HE_6-DNA, and 1.5 ± 0.4 molecules per TP_6/HE_6-DNA.

We had previously shown that the HE_6-DNA conjugate forms micelles with a diameter of ~13 nm.[15] Yet if this polymer is fully stretched, it has an ~7 nm long DNA portion and a ~12 nm long hydrophobic chain. Considering the efficient chain packing of polyethylene[29] and the fact that HE chains are punctuated by phosphate groups, it is possible that they fold upon themselves to enable tight packing between adjacent HE repeats[15] in a similar way to the arrangement of phospholipid bilayers and bola-amphiphiles.[30,31] This would result in a smaller micelle size and a tighter, more densely packed hydrophobic core. The same tight chain packing may be

DOI: 10.1021/jacs.5b12953
J. Am. Chem. Soc. 2016, 138, 4416–4425

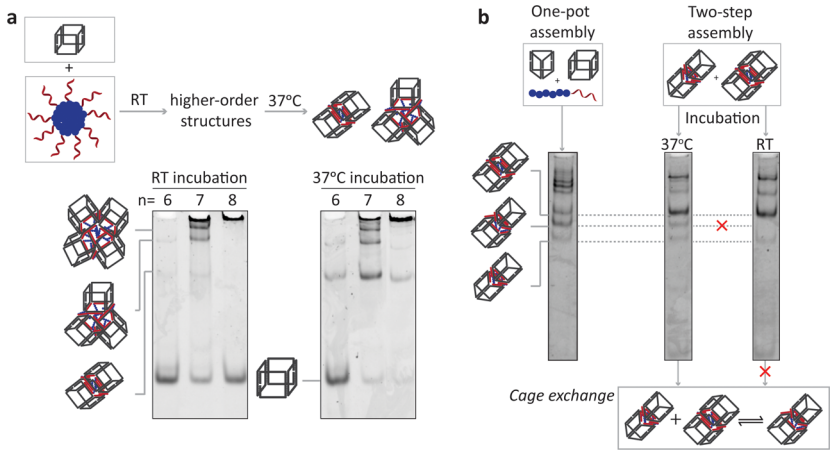

Figure 7. Assembly dynamics of the quantized structures. (a) Mixing of separately preassembled cubes and HE_n-DNA (n = 6–8) micelles generated larger aggregates. Increasing incubation temperature converted these structures back to small structures (dimers, trimers, and tetramers) observed in the one-pot assembly. (b) As representative examples, only the bands corresponding to dimers were labeled. One-pot annealing of TP_3, C_4, and HE_6-DNA generated all cage combinations such as dimers of TP_3/TP_3, TP_3/C_4, and C_4/C_4 (left gel). Mixing separately preformed TP_3/HE_6-DNA and C_4/HE_6-DNA at room temperature did not result in exchange (right gel). Incubation at 37 °C for 30 min resulted in scrambling to the heterodimer (TP_3/C_4).

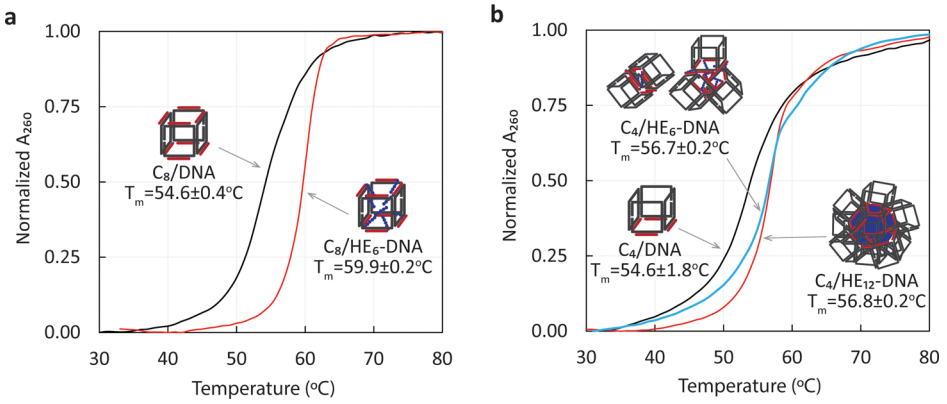

Figure 8. Melting profiles of the assemblies of (a) C_8/DNA and C_8/HE_6-DNA; (b) C_4/DNA, C_4/HE_6-DNA, and C_4/HE_{12}-DNA. An increase in melting temperature (T_m) of the cubes with HE_n-DNA suggested the synergistic stabilization of DNA nanostructures by the hydrophobic interactions. The narrow transition of the curve is consistent with a large increase in cooperativity of DNA hybridization/dissociation in the presence of hydrophobic chains.

present in the core of the "micellar cages" above, which may explain their relatively low loading capacity. It has been shown that the crystallinity of the hydrophobic core of block copolymer micelles tends to decrease the loading capacity for guest molecules, because of lower chain mobility that hinders the diffusion of the hydrophobic molecules.[32−34] While additional studies need to be performed to better understand the chain packing in our "micellar cages", we will also examine reducing the extent of core packing by using unsaturated lipids, rather than HE chains as the hydrophobic units.

Assembly Dynamics and Thermodynamic Properties. The cage architectures described here were all generated by a one-step thermal annealing protocol (95 to 4 °C) where all component strands and DNA polymers were mixed and annealed together. There are two possible mechanisms for their assembly: (i) As the strands are cooled from 95 °C, the cage assembles first, followed by hybridization to the individual DNA–polymer strands; then subsequent hydrophobic interactions drive the assembly of superstructures as the temperature further decreases. (ii) The DNA cage and the micelles preform separately, and the two objects hybridize together into the final structure, thus transitioning from a micelle morphology to cube superstructures. To explore this mechanistic aspect, we preassembled cube C_4 and HE_n-DNA separately and then incubated them together at room temperature for 30 min (see Supplementary Figure 58). Short HE chains (HE_1-DNA to HE_4-DNA) that are not expected to form stable micelles yielded monomeric structures similar to the one-pot assembly. On the other hand, the two-step assembly process with longer chains (HE_6-DNA to HE_{12}-DNA) resulted in nonpenetrating bands, as well as an unfunctionalized DNA cube (Figure 7a and see Supplementary Figure 58). Thus, in this case, the cube cannot disassemble preformed micelles in order to hybridize with their individual chains at room temperature. Interestingly for HE_7-DNA and HE_8-DNA, increasing the incubation temperature to 37 °C converted the mixture of higher-order structures and cube into the cube dimers and trimers observed earlier (Figure 7a and see Supplementary Figures 59 and 60 for temperature dependence). At this temperature, the HE chains in the micelle may possibly rearrange into the more thermodynamically favorable cube-aggregate state. Thus, a preformed DNA–polymer spherical micelle can shape shift into

DOI: 10.1021/jacs.5b12953
J. Am. Chem. Soc. 2016, 138, 4416–4425

quantized cage assemblies, merely by adding DNA cages at 37 °C.

The second question that we would like to address is the possibility of shape discrimination, i.e., whether two DNA cages of the same geometry would prefer to associate together via hydrophobic interactions. In a one-pot annealing of HE_6-DNA with both the trigonal prism TP_3 and cube C_4 strands, we found no selectivity in the cage structures: for example, homo- and heterodimer combinations of TP_3-TP_3, TP_3–C_4, and C_4–C_4 were observed (Figure 7b, left gel). However, if TP_3–TP_3 and C_4–C_4 homodimers were separately generated and mixed together at room temperature for 30 min, no observable exchange occurred (Figure 7b, right gel). At 37 °C, scrambling started to happen (Figure 7b, middle gel). Additionally, we verified the formation of this heterodimer by labeling each of the cube C_4 and trigonal prism TP_3 with two dyes of different emission colors, and observing colocalization by gel electrophoresis imaging (see Supplementary Figure 64). Because of its stability at room temperature, it is possible to isolate the heterodimer (for example, TP_3–C_4) to generate anisotropic nanoparticles, whose free single-stranded faces can be of different sequences and can provide unique sites for further functionalization.

Decoration of HE_6-DNA on the cube C_8 with eight binding sites resulted in a totally different mode of HE chain interactions, as compared to cube C_4. Here, the preorganization of eight HE_6 chains on C_8 increased the extent of the intrascaffold "handshake" of these chains over the interscaffold "handshake". This is likely due to the lower entropic penalty of the intramolecular assembly, and the increase in the effective concentration of HE_6 in the DNA cage core, thus favoring micellization below the critical micelle concentration of the polymers.[15] Thermal denaturation analysis was performed to investigate the thermodynamic properties of these "micellar cages". Interestingly, the presence of HE_6 chains in the core of the cube provided significant stabilization of C_8/DNA, with an increase of 5.5 °C in thermal denaturation (Figure 8a). The full width at half-maximum (fwhm) determined from the first derivatives of the melting curves can be used as the indication for the degree of cooperativity.[35,36] The dramatic decrease in fwhm of C_8/HE_6-DNA (4.0 ± 0.1 °C) in comparison to C_4/DNA (10.1 ± 1.0 °C) indicated a significantly increased positive cooperativity of DNA nanostructure assembly/disassembly. To confirm this cooperativity, we performed a titration experiment, in which increasing quantities of HE_6-DNA were added to C_8 (see Supplementary Figure 56). All-or-none binding was observed with substoichiometric amounts of the DNA polymer with respect to the cube binding sites. On the other hand, titration of C_8 with unmodified DNA strands gave intermediate structures and did not exhibit such a cooperativity (see Supplementary Figure 56). Thus, with the intrascaffold "handshake", the DNA base-pairing and hydrophobic effects are acting synergistically, providing greater stability and assembly cooperativity to the cube-micelle structures. This is of significant importance for the biological applications of these structures.

We hypothesized that decoration of HE_6-DNA on only one face of the cage (C_4) would not affect DNA hybridization to the same extent. C_4/HE_6-DNA exhibited a slight increase of 2 °C in T_m compared to C_4/DNA (Figure 8b). Interestingly, increased cooperativity was also observed in this system, as indicated by a significant decrease in fwhm (10.3 ± 1.8 °C for C_4/DNA and 4.5 ± 0.7 °C for C_4/HE_6-DNA). A comparable increase in T_m and decrease in fwhm was observed for C_4/HE_{12}-DNA. Moreover, some extra stabilization was also observed in assemblies with block HE/HEG-DNA copolymers. Hence, the hydrophobic HE chains contribute to greater stabilization and cooperativity for DNA assemblies; this additional stabilization possibly stems from some additional intrascaffold interactions between HE chains, providing extra cohesion to the assembly. Therefore, the hydrophobic interactions can not only introduce new DNA assembly modes but also synergistically work together with the base-pairing interactions to form and stabilize the DNA nanostructures.

CONCLUSION

We have demonstrated the use of sequence-defined hydrophobic polymers to provide orthogonal assembly modes to DNA cages and to synergistically work together with base-pairing interactions. A range of new structures can be accessed by fine-tuning of the length of hydrophobic blocks, the sequence order of the polymers, and the orientation of the polymers on the cages. Short hydrophobic chains result in monomeric DNA cage structures that are decorated with alkyl or oligoethylene glycol units. Longer hydrophobic chains arranged on one face of the DNA prismatic cage result in quantized cube higher-order structures; here, the number of hydrophobic repeats defines the number of DNA cages that form these aggregates. When these hydrophobic chains are organized on both faces of the cage, these chains point to the interior of the cage and undergo an intrascaffold "handshake". The sequence order of hydrophobic and hydrophilic monomers on the polymer chains can significantly control the interactions between hydrophobic blocks, resulting in monomeric cages and "doughnut-shaped" DNA cage-ring structures for specific sequences. These DNA–polymer nanostructures can be alternatively viewed as amphiphilic block copolymers, where the hydrophilic block consists of a DNA cage and the hydrophobic block has hexaethylene chains. However, unlike block copolymers, the two components are monodisperse and sequence defined, and the placement of hydrophobic polymers on the DNA cage is anisotropic. This gives rise to entirely new morphologies that are not observed with block copolymers and provides guidelines for the design of DNA nanostructures mediated by hydrophobic interactions. It is remarkable that high specificity is achieved in these assembled structures despite the fact that the hydrophobic effect is one of the least directional supramolecular interactions. We have only worked with hydrophobic interactions so far, but the potential for structural complexity and protein-inspired folding is tremendous when additional interactions (fluorophilic, metal binding, etc.) are introduced.

ASSOCIATED CONTENT

Supporting Information

The Supporting Information is available free of charge on the ACS Publications website at DOI: 10.1021/jacs.5b12953.

DNA cage design and assembly, determination of cage aggregation number, gold nanoparticle labeling, characterization by DLS, AFM, and TEM, Nile red encapsulation, studies of stability and cooperativity, effect of cage geometry and concentration, isolation of cage aggregates (PDF)

DOI: 10.1021/jacs.5b12953
J. Am. Chem. Soc. 2016, 138, 4416–4425

AUTHOR INFORMATION

Corresponding Author

*hanadi.sleiman@mcgill.ca

Notes

The authors declare no competing financial interest.

ACKNOWLEDGMENTS

The authors thank NSERC, CFI, CSACS, CIHR, and FQRNT for funding. H.F.S. is a Cottrell Scholar of the Research Corporation. We thank Dr. Alexander Wahba for his help with MS characterization.

REFERENCES

(1) Lutz, J.-F.; Ouchi, M.; Liu, D. R.; Sawamoto, M. *Science* **2013**, *341*, 1238149.
(2) Aldaye, F. A.; Palmer, A. L.; Sleiman, H. F. *Science* **2008**, *321*, 1795.
(3) Winfree, E.; Liu, F.; Wenzler, L. A.; Seeman, N. C. *Nature* **1998**, *394*, 539.
(4) Yan, H.; Park, S. H.; Finkelstein, G.; Reif, J. H.; LaBean, T. H. *Science* **2003**, *301*, 1882.
(5) Liu, D.; Wang, M.; Deng, Z.; Walulu, R.; Mao, C. *J. Am. Chem. Soc.* **2004**, *126*, 2324.
(6) He, Y.; Chen, Y.; Liu, H.; Ribbe, A. E.; Mao, C. *J. Am. Chem. Soc.* **2005**, *127*, 12202.
(7) Chen, J. H.; Seeman, N. C. *Nature* **1991**, *350*, 631.
(8) Rothemund, P. W. *Nature* **2006**, *440*, 297.
(9) Aldaye, F. A.; Sleiman, H. F. *J. Am. Chem. Soc.* **2007**, *129*, 13376.
(10) McLaughlin, C. K.; Hamblin, G. D.; Aldaye, F. A.; Yang, H.; Sleiman, H. F. *Chem. Commun.* **2011**, *47*, 8925.
(11) Wei, B.; Dai, M.; Yin, P. *Nature* **2012**, *485*, 623.
(12) Mai, Y.; Eisenberg, A. *Chem. Soc. Rev.* **2012**, *41*, 5969.
(13) Woo, S.; Rothemund, P. W. K. *Nat. Chem.* **2011**, *3*, 620.
(14) Edwardson, T. G.; Carneiro, K. M.; McLaughlin, C. K.; Serpell, C. J.; Sleiman, H. F. *Nat. Chem.* **2013**, *5*, 868.
(15) Edwardson, T. G.; Carneiro, K. M.; Serpell, C. J.; Sleiman, H. F. *Angew. Chem., Int. Ed.* **2014**, *53*, 4567.
(16) Chen, Y.-J.; Groves, B.; Muscat, R. A.; Seelig, G. *Nat. Nanotechnol.* **2015**, *10*, 748.
(17) Bujold, K. E.; Fakhoury, J.; Edwardson, T. G. W.; Carneiro, K. M. M.; Briard, J. N.; Godin, A. G.; Amrein, L.; Hamblin, G. D.; Panasci, L. C.; Wiseman, P. W.; Sleiman, H. F. *Chem. Sci.* **2014**, *5*, 2449.
(18) Hamblin, G. D.; Carneiro, K. M.; Fakhoury, J. F.; Bujold, K. E.; Sleiman, H. F. *J. Am. Chem. Soc.* **2012**, *134*, 2888.
(19) Fakhoury, J. J.; McLaughlin, C. K.; Edwardson, T. W.; Conway, J. W.; Sleiman, H. F. *Biomacromolecules* **2014**, *15*, 276.
(20) Lee, H.; Lytton-Jean, A. K. R.; Chen, Y.; Love, K. T.; Park, A. I.; Karagiannis, E. D.; Sehgal, A.; Querbes, W.; Zurenko, C. S.; Jayaraman, M.; Peng, C. G.; Charisse, K.; Borodovsky, A.; Manoharan, M.; Donahoe, J. S.; Truelove, J.; Nahrendorf, M.; Langer, R.; Anderson, D. G. *Nat. Nanotechnol.* **2012**, *7*, 389.
(21) List, J.; Weber, M.; Simmel, F. C. *Angew. Chem., Int. Ed.* **2014**, *53*, 4236.
(22) Zhou, C.; Wang, D.; Dong, Y.; Xin, L.; Sun, Y.; Yang, Z.; Liu, D. *Small* **2015**, *11*, 1161.
(23) Wilks, T. R.; Bath, J.; de Vries, J. W.; Raymond, J. E.; Herrmann, A.; Turberfield, A. J.; O'Reilly, R. K. *ACS Nano* **2013**, *7*, 8561.
(24) Serpell, C. J.; Edwardson, T. G.; Chidchob, P.; Carneiro, K. M.; Sleiman, H. F. *J. Am. Chem. Soc.* **2014**, *136*, 15767.
(25) Ko, S.; Liu, H.; Chen, Y.; Mao, C. *Biomacromolecules* **2008**, *9*, 3039.
(26) Walsh, A. S.; Yin, H.; Erben, C. M.; Wood, M. J. A.; Turberfield, A. J. *ACS Nano* **2011**, *5*, 5427.
(27) Buckhout-White, S.; Ancona, M.; Oh, E.; Deschamps, J. R.; Stewart, M. H.; Blanco-Canosa, J. B.; Dawson, P. E.; Goldman, E. R.; Medintz, I. L. *ACS Nano* **2012**, *6*, 1026.
(28) Greenspan, P.; Mayer, E. P.; Fowler, S. D. *J. Cell Biol.* **1985**, *100*, 965.
(29) Ehrenstein, G. W.; Theriault, R. P. *Polymeric materials: structure, properties, applications*; Hanser Publications: Munich; Cincinnati, OH, 2001.
(30) Fuhrhop, J.-H.; Wang, T. *Chem. Rev.* **2004**, *104*, 2901.
(31) Blume, A.; Drescher, S.; Meister, A.; Graf, G.; Dobner, B. *Faraday Discuss.* **2013**, *161*, 193.
(32) Shuai, X.; Ai, H.; Nasongkla, N.; Kim, S.; Gao, J. *J. Controlled Release* **2004**, *98*, 415.
(33) Glavas, L.; Odelius, K.; Albertsson, A.-C. *Polym. Adv. Technol.* **2015**, *26*, 880.
(34) Gou, J.; Feng, S.; Xu, H.; Fang, G.; Chao, Y.; Zhang, Y.; Xu, H.; Tang, X. *Biomacromolecules* **2015**, *16*, 2920.
(35) Eryazici, I.; Prytkova, T. R.; Schatz, G. C.; Nguyen, S. T. *J. Am. Chem. Soc.* **2010**, *132*, 17068.
(36) Greschner, A. A.; Toader, V.; Sleiman, H. F. *J. Am. Chem. Soc.* **2012**, *134*, 14382.

DOI: 10.1021/jacs.5b12953
J. Am. Chem. Soc. 2016, 138, 4416−4425